# Novel Speed and Current Sensor FDI Schemes with an Improved AFTC for Induction Motor Drives

*Mohamed BOUAKOURA, Nasreddine NAIT-SAID, Mohamed-Said NAIT-SAID, Adel BELBACH*

LSP-IE'2000 Laboratory, Electrical Engineering Department, Faculty of Technology, University of Batna 2, Rue Chahid Mohamed El-Hadi Boukhlouf, 05000 Batna, Algeria

bouakouramohamed@gmail.com, n_naitsaid@yahoo.com, medsnaitsaid@yahoo.fr, adel.belbach@hotmail.fr

DOI: 10.15598/aeee.v16i1.2573

***Abstract.*** *This paper focuses on speed and current sensor Faults Detection and Isolation (FDI) in an Induction Motor (IM) drive. The effect of sensors faults on the IM vector control is presented, then, new detection and isolation approaches are suggested. Speed sensor faults are detected when an error between only two points from speed data exceeds a certain threshold. An algorithm based on RMS currents is developed to detect and isolate any faulty current sensor. This requires three current sensors, each per phase. Besides, open circuit faults of inverter power switches are taken into account too. To ensure continuous functionality of the drive, we conceived an Active Fault Tolerant Controller (AFTC) with smoother reconfiguration feature. Simulations in Matlab/Simulink are carried out to show the efficiency of the suggested schemes.*

## Keywords

***Active fault tolerant control, current sensor, inverter power switch, MRAS, RMS value, speed sensor.***

## 1. Introduction

Fault Tolerant Control (FTC) is a technique implemented in many critical and high availability systems. Its main purpose is to mitigate faults and ensure a continuous functionality of a system with faulty elements rather than total failure. The first FTC was implemented in aircrafts [1]. After that, it has been broadened to many other fields, such as power plants [2], transportation [3], [4] and [5], and wind energy conversion systems [6], [7] and [8]. To control any process, accurate feedback information is required, and this one is provided by sensors. Thus, in this paper, we investigate particularly speed and current sensor faults in an induction motor drive. The choice was taken since induction motor drives are involved in most propulsion and traction applications [9].

Fault tolerant techniques are divided into two types: passive FTCs and active FTCs. The first ones involve robust controllers such as H_$\infty$ [10] and [11] and sliding mode controllers [12], [13] and [14], i.e. the faulty element remains integrated in the system where the controller absorbs its effect. Nevertheless, this technique has a limited effectiveness because it tolerates only low severity faults [15] and [16]. Active FTCs (AFTC), or reconfigurable FTCs, are more suitable for severe faults since the faulty component is replaced automatically by a healthy one or its signal is generated by a mathematical model based on other available sensors. AFTC necessitates a Fault Detection and Isolation (FDI) mechanism.

In some papers, hardware redundancy is considered for fault detection [17] and [18], whereas in others analytical redundancy is preferred. This last rely on estimators and observers, for example; in [19] an extended Kalman filter is considered as a speed virtual sensor. Alkaya and Eker applied a Luenberger observer with a DC motor to detect speed sensor faults [20]. MRAS is also a widely used method for speed estimation. It is presented by Wang et al. as a substitute for the faulty speed sensor [21]. Usually, when it is hard to model a process, signal processing and machine learning approaches are effective. In [22], wavelet analysis has a fundamental role in FTC scheme. In [23] the authors considered the stator current signature as a reliable tool to detect eccentricity faults of induction motors. Fuzzy logic was an efficient tool used by Kamal et al. to estimate sensor faults in a wind-diesel hybrid system [24] and also in [25] to develop a more efficient control for an induction motor.

Many researchers dealt with sensors faults. In [7], [26] and [27] sensors malfunction causes significant loss of the controller performance. Hence, this issue was a motivation to FTC design. This paper covers several contributions to speed and current sensor faults diagnosis and tolerance in induction motor drives. First, the effect of sensors faults on the IM vector control (IFOC) is presented. Then, we propose new detection and isolation strategies based on signal processing. Last mentioned are effective and easy to implement. To handle these faults, an improved AFTC scheme is developed with smoother reconfiguration feature at sensor fault moment.

This paper is organized as follows: Section 2. is dedicated to the detection and isolation of speed and current sensor faults. Section 3. presents an extension of current sensor FDI algorithm to detect and isolate inverter leg open switches faults. The main improvements on the AFTC are explained in Sec. 4. Section 5. concludes the paper.

**Remark 1.** *Note that in Fig. 2, Fig. 5, Fig. 6, Fig. 8, Fig. 11 and Fig. 12 the rectangle with rounded angles represents a conditional test. Its output is binary, so it equals "1" if the condition is verified, otherwise it equals "0".*

# 2. Speed and Current Sensor Fault Diagnosis

Before we present the FDI algorithms, we show the influence of speed and current sensor faults on the performance of the IM drive with indirect field-oriented control. We chose it since it is one of the most performant and widespread technique.

The intermittent fault in speed sensors of DC generator type or alternators is usually caused by rotor eccentricity [28] and [29] or the attrition of brushes or bearings. Whereas offset faults may be caused by the variation of electrical parameters of the sensor in some operating conditions. In rotary encoders, an insufficient light source (LED) or a malfunction of the phototransistor produces uncertain measurement [8] and [29]. The mechanical sliding in both types of speed sensors (encoder, generator) causes abrupt changes in measurement.

Since IFOC controls motor currents, the last mentioned are usually measured by at least two current sensors, but sometimes they are estimated from speed and DC bus voltage. To increase the reliability of the drive we prefer to measure phase currents instead of estimating them relying on other sensors.

Current sensor faults are less severe than those of speed sensor, yet, they alter the controller performance. The causes of current sensor malfunction are related to its physical structure. In some functioning conditions, the change in material properties and also the degradation after a long time of use produces sensor faults. Current sensors based on Hall effect are not linear with respect to magnetic flux density, so they may be saturated if the measured current exceeds the nominal supported value, which engenders a bias in measurement [30] and [31]. A disconnection of the electrical link or breakdown of the sensor is an origin of the total loss of feedback information.

**Remark 2.** *In all simulations in this section, rated load toque $Tl = 6.1$ [Nm] is applied at $t = 1$ [s] and each fault is activated at $t = 1.5$ [s].*

## 2.1. Speed Sensor Faults Effect on IFOC

In this paper, the investigated faults are: intermittent fault, offset fault, and total loss fault. Each one is performed in Matlab as follows:

$$\begin{cases} \text{Intermittent fault:} & \Omega_f = \Omega + \delta, \\ \text{Offset fault:} & \Omega_f = \Omega + \gamma, \\ \text{Total loss:} & \Omega_f = \Omega \times 0, \end{cases} \tag{1}$$

where $\gamma$ is the offset value, $\gamma = 10$ rad·s$^{-1}$, and $\delta$ is a random number with a mean value equal to 0 and a variance equal to 10 rad·s$^{-1}$.

Figure 1 shows phase current, rotor fluxes on "dq" reference frame, and speed for each speed sensor fault. Speed sensor faults have a clear impact on the vector control. The intermittent fault causes significant torque ripples which cause the changes in speed (Fig. 1(a)). Regarding offset fault (Fig. 1(b)), it is treated almost as a load torque by the vector control. So the phase currents rise instantly. However, the effect of the fault on the actual speed is not eliminated since the offset value added to the actual speed makes the speed value provided by the faulty sensor equal to the reference. Total loss fault is the most risky because the speed becomes no longer controlled. Thus, we limited the stator electric speed "$\omega_s$" and the current "$I_{sq}$" to prevent speed divergence. Stator currents rise to two times the rated current at the fault moment and rotor fluxes do not follow their references after the fault (Fig. 1(c)). The Torque ripple rate increases to $Te_{\max-\min} \approx 5.8$ Nm.

## 2.2. Speed Sensor Faults Detection

Most often, the speed variation due to a sensor fault is faster than its variation due to a torque load, change in speed reference or faults in other components of the

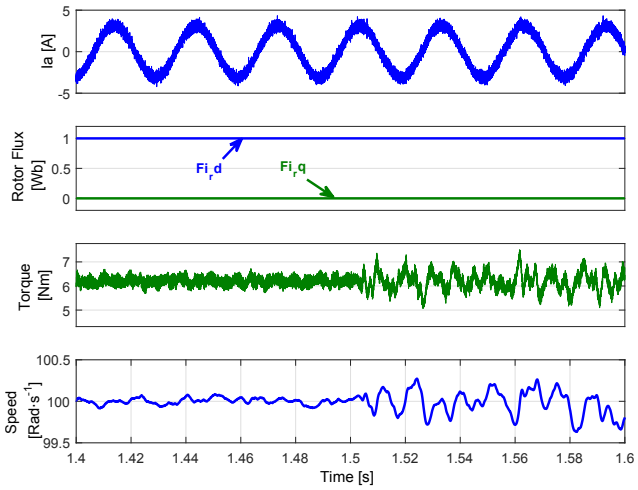


(a) Intermittent fault.

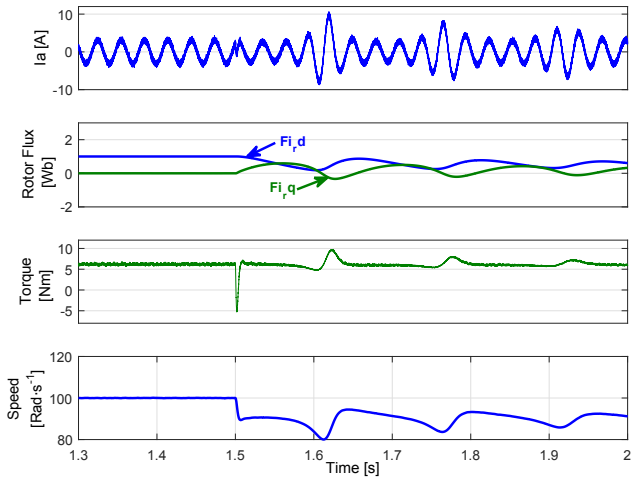


(b) Offset fault.

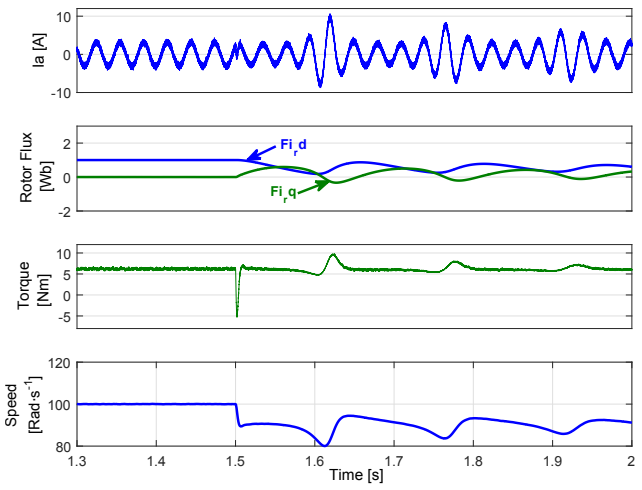


(c) Total loss fault.

**Fig. 1:** Phase current, rotor fluxes on "dq" reference frame, and actual speed in presence of speed sensor fault: (a) intermittent fault, (b) offset fault, (c) total loss fault. With $\Omega^* = 100$ rad·s$^{-1}$, $Tl = 6.1$ Nm and $\phi_r^* = 1$ Wb. Each fault is applied at $t = 1.5$ s.

drive [32]. From this standpoint, the detection could be achieved by comparing only two points from speed data between which the distance is proportional to the sampling time. In our case, since $T = 5 \cdot 10^{-6}$ s , five steps distance is sufficient; $\tau_d = 5 \times T$. The detection signal is computed as illustrated by the scheme in Fig. 2. This proposed speed sensor faults detection scheme is less runtime consuming compared to observer based approaches or some simple signal processing techniques such as average standard deviation in [32].

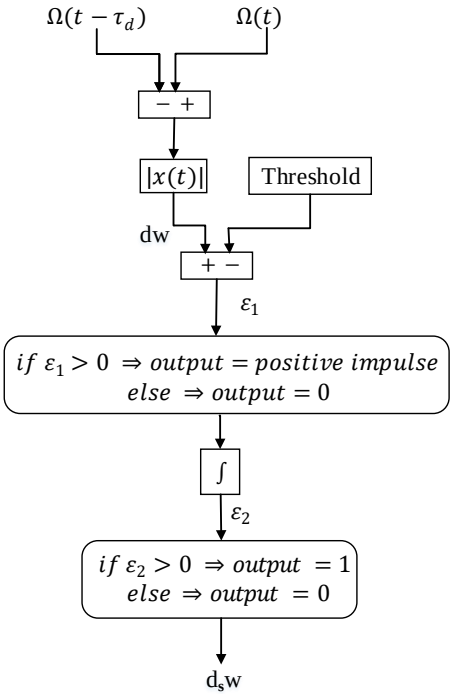


**Fig. 2:** Detection scheme of speed sensor faults. With $\tau_d = 5 \times T$.

Figure 3 shows the simulation results for the suggested detection method with three different faults. It is clear that any abrupt change in speed data generates impulses in "$d\omega$" curve.

Hence, any impulses due to measurement noise, load torque or transients in speed are kept under a preset threshold. At fault occurrence moment, "$d\omega$" exceeds the threshold generating a detection signal "$ds\omega$". The difference between "$d\omega$" and the threshold is represented by "$\epsilon_1$". When its value is greater than zero, we get an impulse which is then integrated to get a constant signal "$\epsilon_2$". Since this value is very small, it is transformed via a relay to produce a meaningful binary signal.

## 2.3. Current Sensor Faults Effect on IFOC/Sensorless IFOC

Three different faults are considered; offset fault, gain fault, and total loss of feedback information. They are

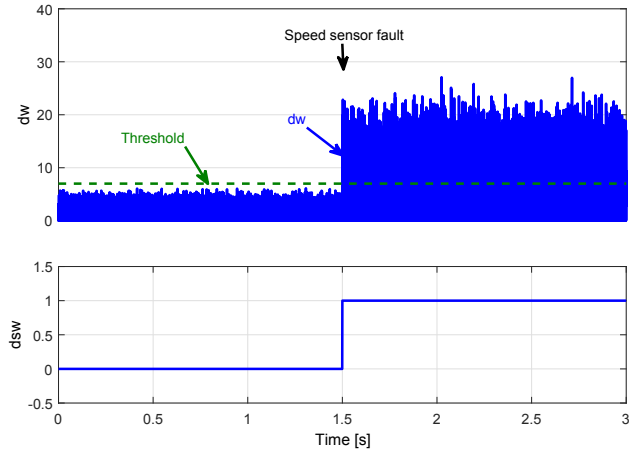


(a) Intermittent fault.

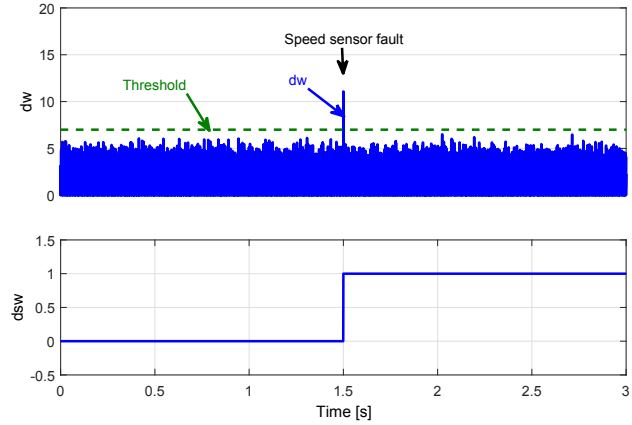


(b) Offset fault.

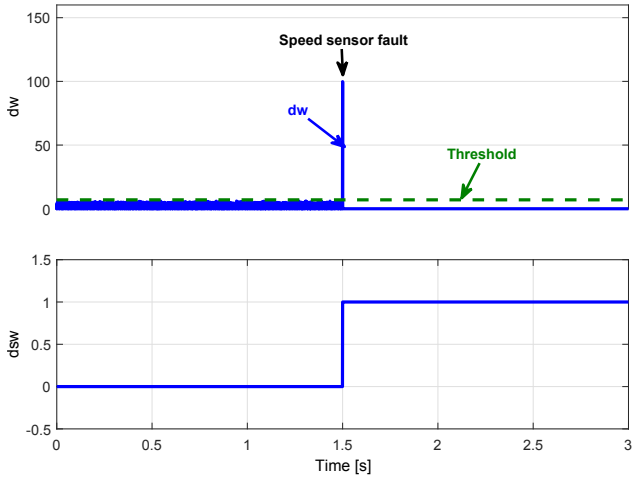


(c) Total loss fault.

**Fig. 3:** Detection results of speed sensor faults: (a) intermittent fault, (b) offset fault, (c) total loss fault.

simulated in Matlab as follows:

$$\begin{cases} \text{Offset fault:} & I_{cf} = I_c + \rho, \\ \text{Gain fault:} & I_{cf} = I_c \times \varpi, \\ \text{Total loss:} & I_{cf} = I_c \times 0, \end{cases} \tag{2}$$

where $\rho$ is the offset value ($\rho = 2A$) and $\varpi$ is the gain coefficient ($\varpi = 0.5$).

The offset value and the gain are chosen relatively small, so they will not have a considerable impact on electrical and mechanical variables, yet, they should be detected by an algorithm (software) using the measurements of other non-faulty sensors. In the case of IFOC with speed encoder, current sensor faults cause either fluctuation of rotor fluxes (offset fault) or deviate them from their references (gain and total loss fault). Consequently, considerable torque oscillations are noticed with $Te_{\max-\min} \approx 5$ Nm, which may lead to long-term to a mechanical deterioration of the shaft. In sensorless operation, MRAS speed estimator loses its efficiency when current sensors provide inaccurate values. Hence, this leads to a total controller failure.

Figure 4 illustrates: "$I_b$" phase current, rotor fluxes on "dq" reference frame, torque, and speed. We chose to simulate the fault of only one current sensor since the occurrence probability of two or three faults in a short time period is very low. Both operations are considered: with and without a speed sensor.

## 2.4. Faulty Current Sensor Detection and Isolation

The simplest way to detect a current sensor fault in a balanced three-phase system is the sum of the three currents. This sum is practically null in normal operation of the drive, yet it changes due to a current sensor fault. We adopted the absolute mean value of three currents sum "$I_f$" as a fault indicator "$d_s i$" when it exceeds certain threshold "$\zeta$" (Fig. 5). As for localization, a new algorithm is proposed based on RMS values of phase currents. The use of RMS values permits the localization of a current sensor under gain fault, unlike average values which are null when currents still alternating after the fault. Hence, the efficiency of the technique proposed in [7] is not verified with gain fault. Moreover, the developed method in this paper is less computationally demanding than the one in [7].

The key idea of localization is to look for the minimum value between two RMS values of phase currents. Because this value corresponds to the difference between the RMS currents measured by healthy sensors, then the remaining phase current is measured by a faulty one. From Fig. 6, if the sensor of phase "$b$" is faulty, $r_b$ will be equal to "0" since it is the difference between the value chosen by the function minimum and the difference $|I_{a_{rms}} - I_{b_{rms}}|$. When $r_b = 0$, then the conditional test is verified and the middle output will be equal to "1". This latter is multiplied by 2 which is the index of phase "$b$". Since *faulty sensor index* is not constant before the fault occurrence we multiply it by "$d_s i$" to avoid any false localization signal. The

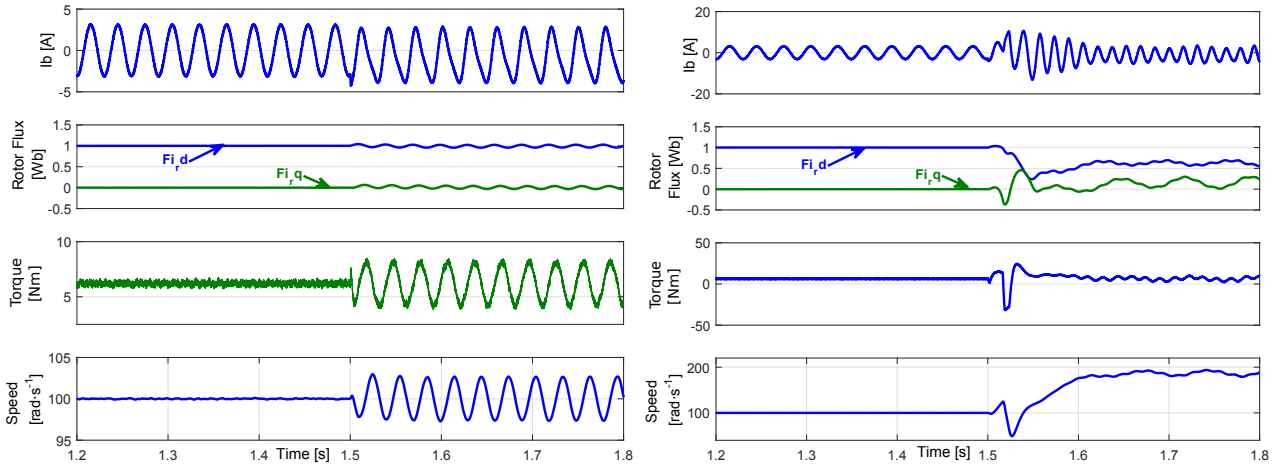


(a) Offset fault.




(b) Offset fault with MRAS.

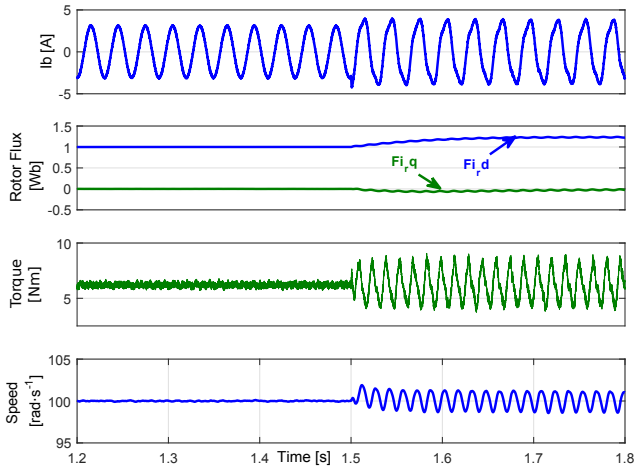


(c) Gain fault.

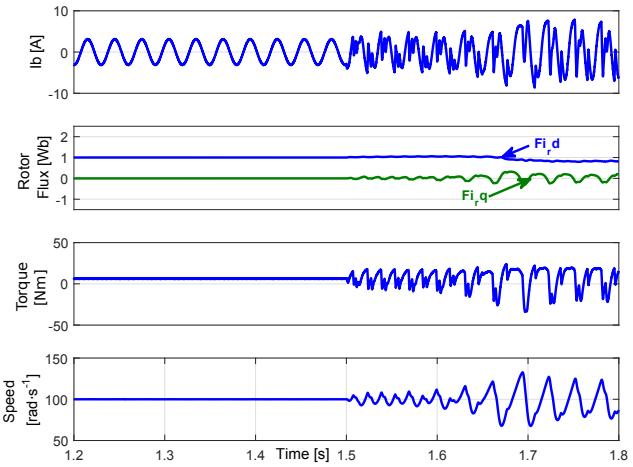


(d) Gain fault with MRAS.

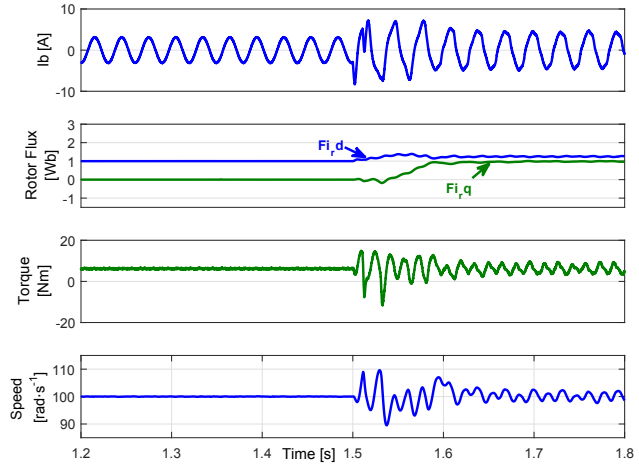


(e) Total loss fault.

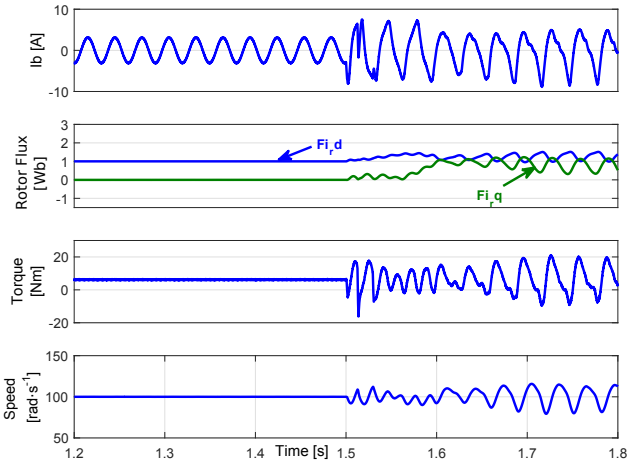


(f) Total loss fault with MRAS.

**Fig. 4:** Phase current, rotor fluxes on "dq" reference frame, torque and actual speed in presence of current sensor fault of phase "b" with speed sensor and with MRAS. $\Omega^* = 100$ rad·s$^{-1}$, $Tl = 6.1$ Nm and $\phi_r^* = 1$ Wb. Each fault is applied at $t = 1.5$ s.

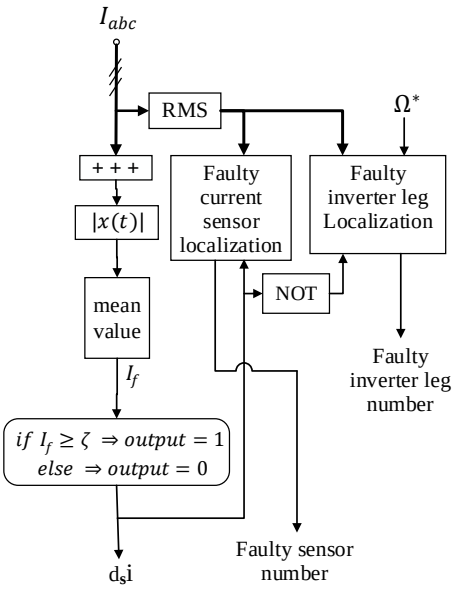


**Fig. 5:** Global block scheme of current sensor/inverter leg fault detection and isolation.

proposed algorithms are verified by simulation and the results are shown in Fig. 7. For all three considered faults, the gap between the RMS values corresponding to healthy sensors is the smallest. Faulty sensor localization block is intentionally activated after 0.035 s from detection moment, which is the time required to get a constant localization signal.

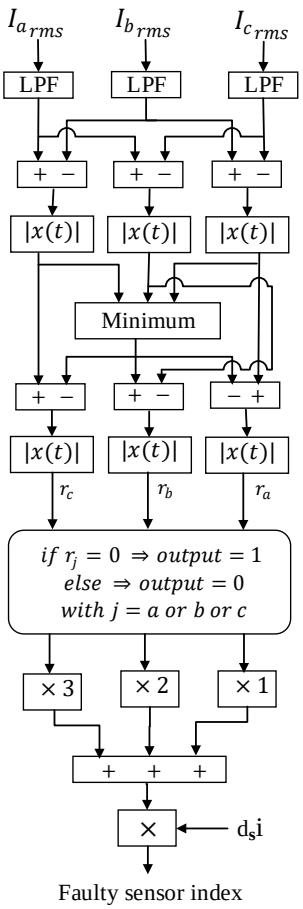


**Fig. 6:** Isolation scheme of faulty current sensor.

## 3. Faulty Power Switch Detection and Localization

As an extension to sensor fault diagnosis, we added a block to identify the inverter leg with a faulty power switch. Short circuit faults of power switches cannot be localized fast enough since the current of the DC voltage source increases in milliseconds to a high value which triggers the protection components (fuse or relay) to shut down the drive. Only open circuit faults of controlled power switches are considered because they are more prone to faults than antiparallel diodes. One-half cycle of phase current passes due to the loss of an inverter power switch. Consequently, the RMS current in faulty inverter leg decreases. Figure 8 shows the algorithm to detect and localize the faulty inverter switch. For example, if top switch of the second leg is open-circuited, the RMS current of the second phase "$I_{b_{rms}}$" will have the lowest value, and the two other RMS currents "$I_{a_{rms}}$" and "$I_{c_{rms}}$" will rise to compensate the current drop. As illustrated in Fig. 8, after the fault, $z_b$ stays in the defined interval: $\rho_{\min} < z_b < \rho_{\max}$ however: $z_a$, $z_c$ vary such as: $\rho_{\max} < z_a$, $\rho_{\max} < z_c$. The difference between the output of the function minimum and $I_{j_{rms}}$ is noted as $z_j$. With $j$ is the phase index and $j = a$ or $b$ or $c$. The interval limits: $\rho_{\min}$, $\rho_{\max}$ are chosen close to zero, where $\rho_{\min} = -0.04$ and $\rho_{\max} = 0.04$. The conditional test output equals one if $z_j$ is included in the interval $[\rho_{\min}, \rho_{\max}]$ otherwise it equals zero. In the considered case, the output of the conditional test block is [1 1 1] before the fault and [0 1 0] after the fault occurrence. When these binary values pass by the NAND function, they generate a detection signal "$d_s ps$" which is null before the fault -in steady state- and equal to 1 after it. Since the antiparallel diode allows the continuity of current, an open switch fault affects slightly the sum of three currents. This is used to differentiate between sensor and power switches faults. We multiply by the inverse of the sensor fault detection signal "$(\overline{d_s i})$" to turn off the localization block of power switches faults when a current sensor fault occurs. Also, to eliminate any false alarm due to different changes in speed reference, we set an adaptive threshold in function of speed reference, where the $\lambda_{ss}$ and $\lambda_{ts}$ are the steady and transient state thresholds respectively. $\lambda_{ts}$ is activated only if the reference speed changes and its derivative is superior to one. The localization of the upper switch fault in the second inverter leg is simulated in Matlab and the result is illustrated in Fig. 9. Notice that in a transient

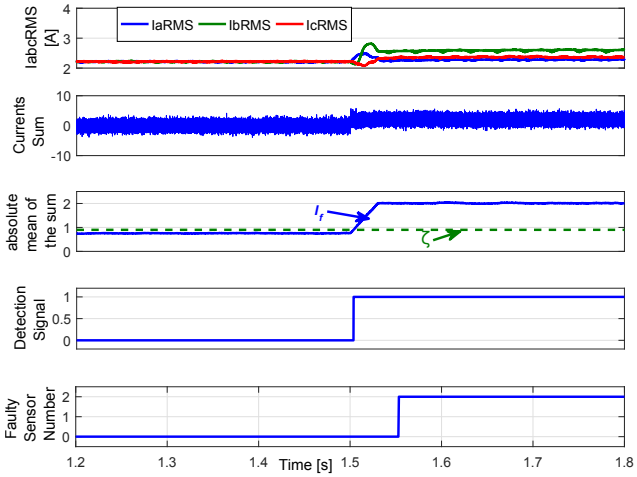


(a) Offset fault.

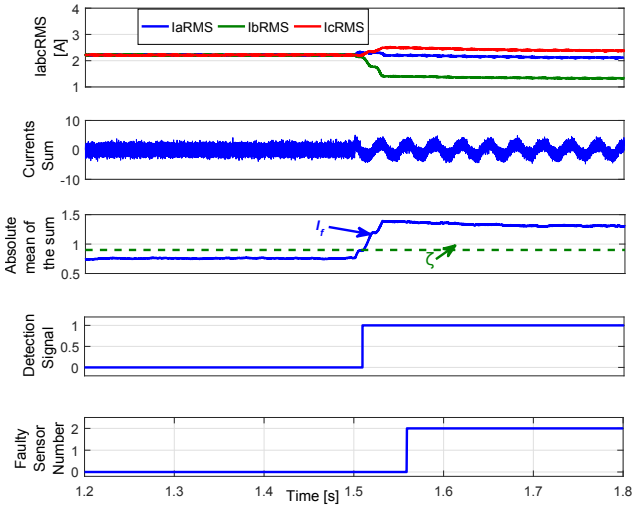


(b) Gain fault.

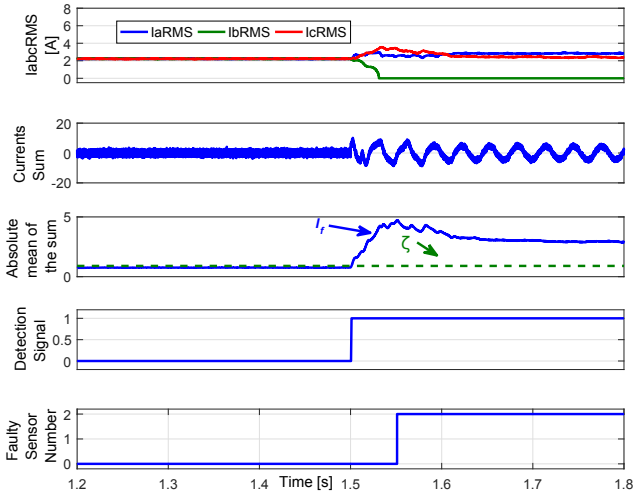


(c) Total loss fault.

**Fig. 7:** Detection and isolation results of current sensor faults: (a) offset fault, (b) gain fault, (c) total loss fault.

state ($0 < t < 0.25$) "$d_sps$" is not null, which could produce a false alarm if we did not use an adaptive threshold. The pre-localization signal "$l_sps$" is activated by "$d_sps$" because it has no meaning until the fault occurrence, where its value indicates the faulty leg.

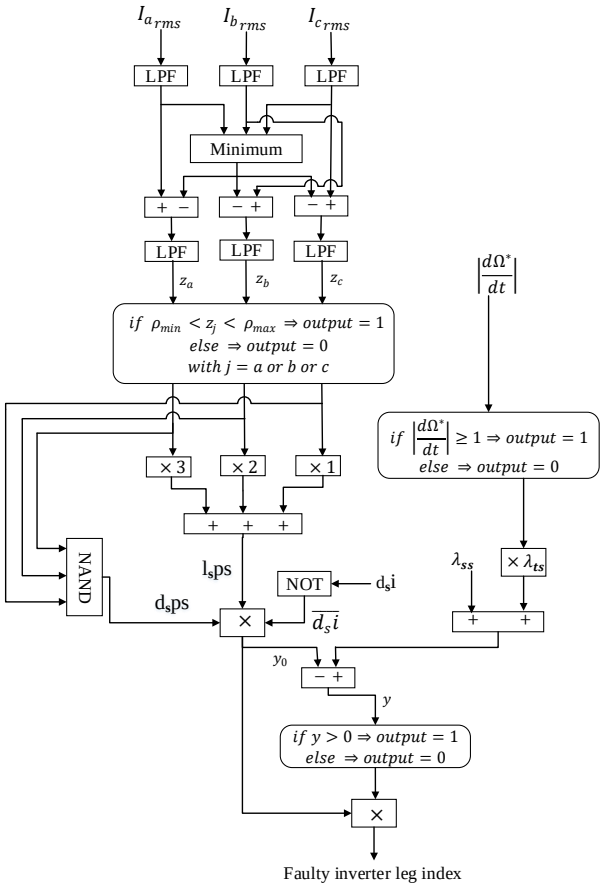


**Fig. 8:** Faulty leg isolation algorithm.

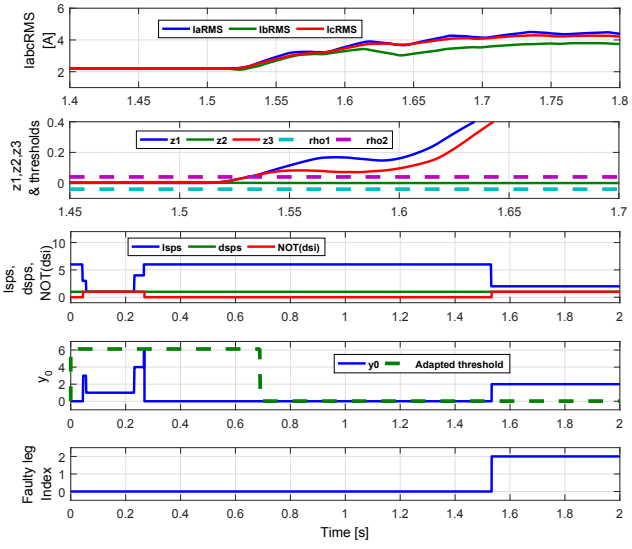


**Fig. 9:** Faulty leg isolation results.

Since no current sensor fault occurred, "$(\overline{d_s i})$" is constantly equal to "1". The detection and localization delay is due to the low pass filters used to reduce signals fluctuations.

# 4. Improved AFTC

## 4.1. Overview of the AFTC Scheme

Figure 10 shows the overall scheme of the IM drive with an AFTC and a detection mechanism. A speed encoder and three current sensors are used for measurement. All sensors data pass by a detection block to detect any sensor malfunction. Reference voltages are generated by the active fault tolerant controller.

The AFTC block incorporates four different control techniques, each one of them requires a certain minimum of sensors to function properly. The selection of the control strategy is achieved automatically depending on the outputs of the sensors faults detector. In Tab. 1, we summarize the possible detector outputs, remaining healthy sensors, and the chosen controller.

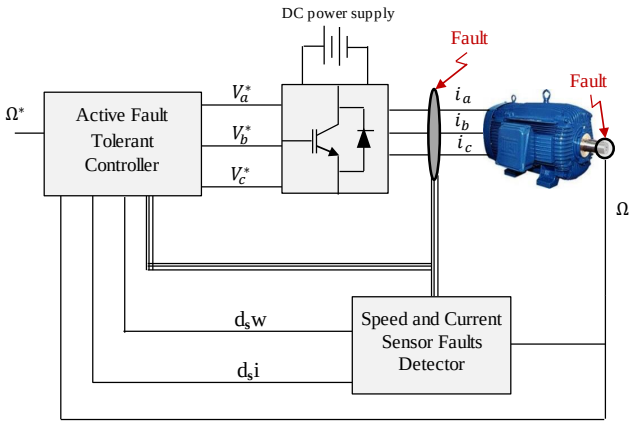


**Fig. 10:** Overall scheme of the IM drive with AFTC.

**Tab. 1:** Detection signals and the selected control technique.

| | $\mathbf{d_s i}$ | $\mathbf{d_s w}$ | **Remaining healthy sensors** |
|---|---|---|---|
| Controller number 1: IFOC | 0 | 0 | Speed sensor, three current sensors |
| Controller number 2: IFOC sensorless | 0 | 1 | Three current sensors, DC voltage measurement |
| Controller number 3: V/f CL | 1 | 0 | Speed sensor |
| Controller number 4: V/f OL | 1 | 1 | No sensors available |

## 4.2. Smoothening the Transition to V/f CL Control

In AFTC, after detecting a sensor fault, a reconfiguration of the control scheme is necessary, but this step is not always straightforward. As shown in Fig. 11, there is a phase shift between the reference voltage of IFOC and V/f CL. Thus, the transition between these two control techniques produces significant torque distortion and considerable speed fluctuation due to a deceleration of the rotating magnetic field.

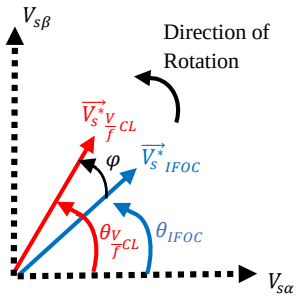


**Fig. 11:** Reference voltage of IFOC and V/f CL on "$\alpha\beta$" reference frame.

Several researchers suggested some ideas to reduce the effect of the transition, for example, Diallo et al. recommend that the switching must be performed when the phase shift between the reference voltages of vector control and scalar control is almost zero [33]. However, in their paper, the selection of the suitable switching moment is not done automatically by the controller but programmed by the authors. In [34], the authors reduced the phase shift between the controllers by readjusting the PI parameters of V/f CL. In these papers, the process from detection to transition is not well clarified. In this section, we present a new approach to smoothen the transition in the AFTC by linking reference voltages of two controllers where one is active and the other is on standby before the transition moment. Then, the controller in standby is liberated gradually to take over when it is selected. Besides, an adaptation of the reference speed is necessary to achieve a better performance.

The new scheme of V/f CL control is shown in Fig. 12. Basically, two main modifications on V/f CL control are done to smoothen the transition to it from IFOC due to a current sensor fault:

- The first modification consists of preparing the controller V/f CL to take over by fixing its reference voltage on IFOC's, i.e. the electric frequencies of the two controllers are equalized. This is performed by the following equation:

$$\omega'_{s_{\frac{V}{f}CL}} = \omega_{s_{\frac{V}{f}CL}} - \left(\omega_{s_{\frac{V}{f}CL}} - \omega_{s_{IFOC}}\right) \cdot R_{cCL}, \tag{3}$$

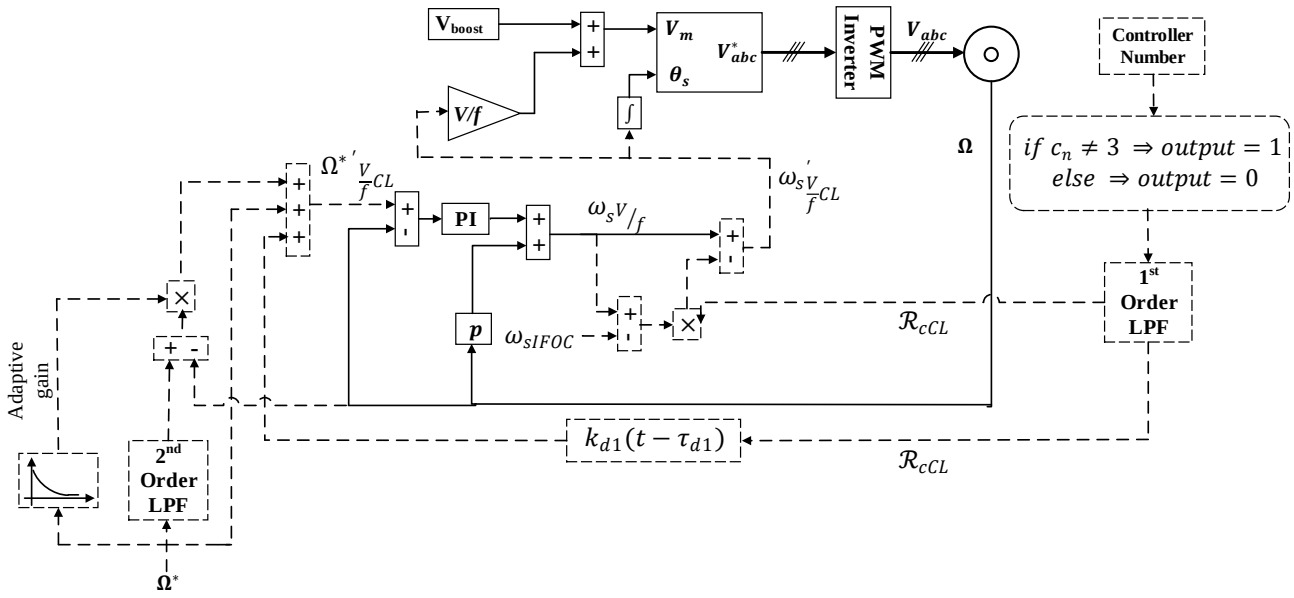


**Fig. 12:** Modified V/f CL control for soft transition. "Dashed line" stands for all the modifications on the basic scheme.

where $\omega'_{s_{\frac{V}{f}CL}}$ is the new electric frequency of V/f CL control. $R_{cCL}$ is the releasing coefficient. It equals to "1" as long as V/f CL controller is not selected. At the transition At the transition moment $R_{cCL}$ goes to "0" gradually through a low pass filter. This means that the V/f CL control becomes independent after transition.

- The second modification consists in adapting $\Omega^*$ by Eq. (4), assumed as an anticipation action, to reduce all sorts of speed deviations from the reference, including speed variation due to transition.

$$\Omega^{*'}_{\frac{V}{f}CL} = (Adaptive\ gain) \cdot \left(\left(2^{nd}\ Order\ LPF\right) \cdot \Omega^* - \Omega\right) + R_{cCL} \cdot k_{d1}\left(t - \tau_{d1}\right), \tag{4}$$

where:

  - $\Omega^{*'}_{\frac{V}{f}CL}$ is the adapted speed reference of V/f CL control.
  - $k_{d1}(t - \tau_{d1})$ permits an instantaneous amplification of speed reference after the switching moment. It is delayed by $\tau_{d1}$ to keep a maximum value for a short time starting from the switching instant.
  - The 2nd order LPF is considered as a reference system. The difference between its output and $\Omega$ is added to the reference speed through the adaptive gain. So, the responses of the IM drive and reference system are intended to be similar. This simple modification brings many advantages, it does not only soften the transition but also improves the dynamic behavior by reducing the overshoot and the effect of the load torque.
  - The adaptive gain is computed in function of $\Omega^*$ using a designed lookup table. This latter is formed of eleven-speed reference points and the corresponding gain values allowing the smoothest transition from IFOC to V/f CL control.

## 4.3. Smoothening the Transition to V/f OL Control

The new scheme of V/f OL control is shown in Fig. 13. Same improvements are made to V/f OL control to smoothen the transition to it from sensorless IFOC or V/f CL.

- $\vec{V}^*_{s_{\frac{V}{f}OL}}$ is linked to $\vec{V}^*_{s_{\frac{V}{f}CL}}$ by Eq. (5):

$$\omega'_{s_{\frac{V}{f}OL}} = \omega_{s_{\frac{V}{f}OL}} + \left(\omega'_{s_{\frac{V}{f}CL}} - \omega_{s_{\frac{V}{f}OL}}\right) \cdot AR_{cOL}, \tag{5}$$

where:

  - $\omega'_{s_{\frac{V}{f}OL}}$ is the new stator electric speed of V/f OL control.
  - $AR_{cOL}$ is an adaptive releasing coefficient. Its value is always equal to "1" till the V/f OL control is selected, then, it transits to "0" gradually through a 1st order LPF with an adaptive time constant "$\tau$". A lookup table is composed of eleven speed reference points and the corresponding "$\tau$" values chosen to allow the smoothest release of $\vec{V}^*_{s_{\frac{V}{f}OL}}$.

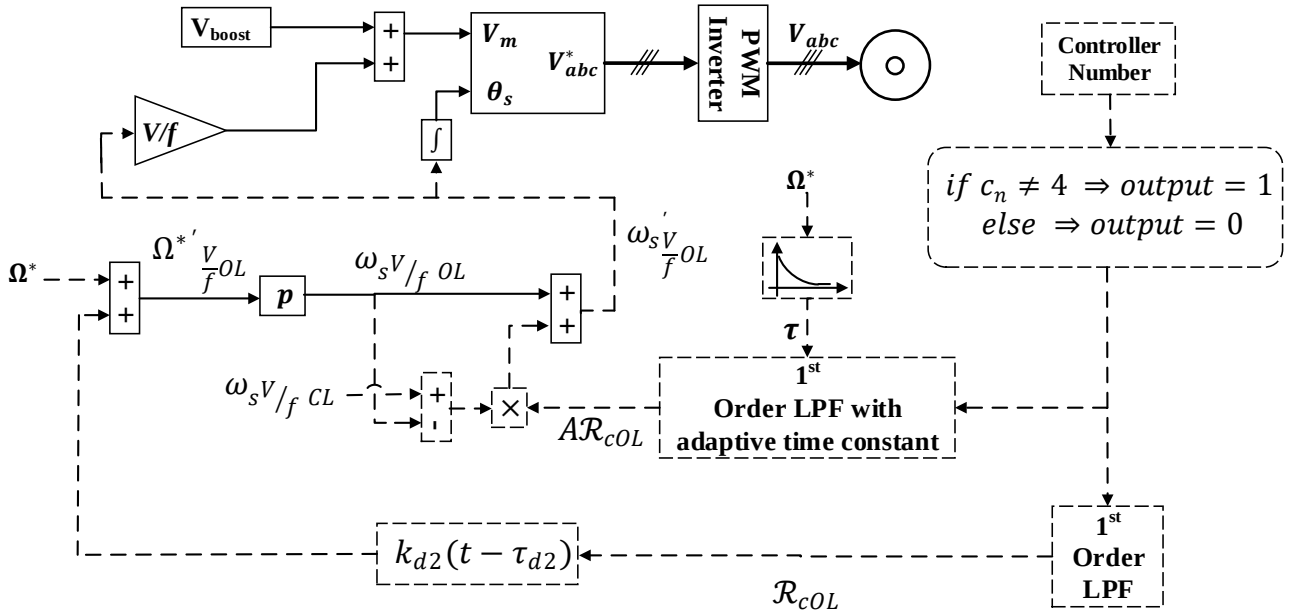


**Fig. 13:** Modified V/f OL control for soft transition. "Dashed line" stands for all the modifications on the basic scheme.

- Reference speed is also adapted according to the following equation.

$$\Omega^{*'}_{\frac{V}{f}OL} = \Omega^* + R_{cOL} \cdot k_{d2}\,(t - \tau_{d2})\,, \qquad (6)$$

with:

  - $\Omega^{*'}_{\frac{V}{f}OL}$ is the adapted speed reference of V/f OL control.
  - $R_{cOL}$ is a releasing coefficient going from "1" to "0" progressively at the switching moment.
  - $k_{d2}\,(t - \tau_{d2})$ is a gain used to boost the value of $\Omega^*$ for a short time starting from the transition moment.

A simulation of the proposal has been carried out in Matlab/Simulink, and the results are illustrated in Fig. 14. The transition was performed at 100 rad·s$^{-1}$ speed reference and with a full load torque $Tl$ = 6.1 Nm. The AFTC with the suggested algorithms exhibits better performance in terms of transition smoothness. Unlike some works in this field, the transition here is performed automatically after the detection of a sensor fault. So, in our case, we choose only the time of sensor fault and the rest is up to the detection and reconfiguration algorithms. Figure 14(a) shows the behavior of the AFTC towards a speed sensor fault followed after two seconds by a current sensor fault. The first fault has almost no effect on the IM drive since its detection is fast and it is mitigated not by changing the controller but only by substituting the faulty speed encoder by the MRAS block. At $t$ = 2 s, a loss of a current sensor is encountered by switching from sensorless IFOC to V/f OL control. This results in an instantaneous current rise, torque ripple, and speed fluctuation. Since the speed is contained in an interval ±15 % of speed reference, the results are quite satisfying.

In Fig 14(b) the scenario is as follows: at $t$ = 1.5 s a current sensor fault occurs, then at $t$ = 3.5 a speed sensor fault occurs as well. In both cases, the transition does not increase overly the phase currents. However, this one engenders some damped torque ripples and speed fluctuations that are also contained in an interval of ±15 % of speed reference. This result is relatively better than the one presented in [34], where the transition is performed on a 7.5 kW motor at 60 rad·s$^{-1}$, and with a light load torque $Tl$ = 5.4 Nm. We point out that speed control of low power IMs is more difficult because of low inertia and high stator winding resistance. Moreover, it is also noticed that both sensor fault detectors are robust, i.e. each responds only to the fault to which it is designed for and it is not affected by faults in other parts of the drive.

## 5. Conclusion

This paper dealt with speed, current sensors, and inverter power switches faults in an induction motor drive. The effect of sensors faults on the vector controller performance is presented and new detection and isolation methods are suggested. Speed sensor faults detector reacts to any abrupt change in speed data. This is achieved by calculating the difference between the last speed value and its value before five simulation steps. To detect currents sensors faults, a detection and isolation algorithm is presented based on the RMS values of phase currents. This algorithm requires

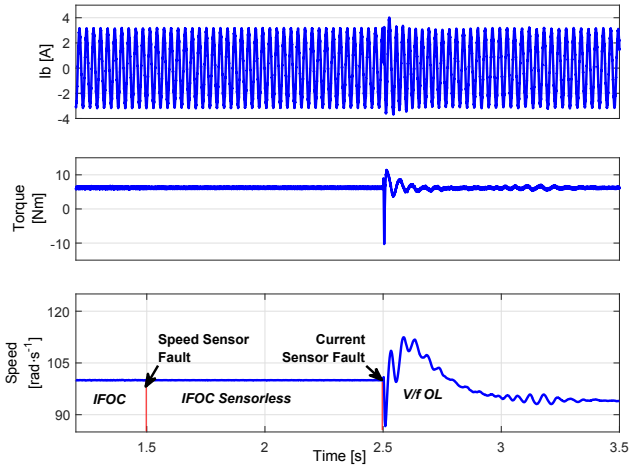


(a) A speed sensor fault, then a current sensor fault.

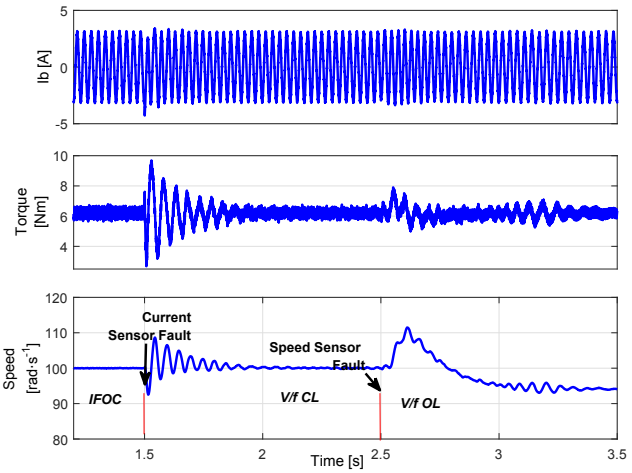


(b) A current sensor fault, then a speed sensor fault.

**Fig. 14:** Control reconfiguration due to: (a) a speed sensor fault, then a current sensor fault, (b) a current sensor fault, then a speed sensor fault. With $\Omega^* = 100$ rad·s$^{-1}$, $Tl = 6.1$ Nm and $\phi_r^* = 1$ Wb.

only three current sensors used for measurement, which makes it more reliable compared to the observer-based approaches. Since currents RMS values are already computed, they serve also for detection and localization of the power switch faults. These simple detection methods are robust towards measurement noise and load torque. Besides, they respond to faults occurrence in less than 0.1 second.

To encounter sensors faults, an active fault tolerant control is developed. It is updated to make the transition between its incorporated control techniques more seamless. The AFTC in this paper starts with a performant control strategy (IFOC) which involves speed and three current sensors, then, as we lose sensors, the AFTC reconfigures its structure till the most basic controller (V/f OL control), where all sensors are faulty.

The experimental validation of the suggested schemes could be carried out by Matlab and dSPACE interface. All faults can be performed on computer by modifying the measurement signals provided by sensors. For example, at a given moment, to activate an intermittent fault, we multiply the measured value by a random signal on the computer. The detection and control schemes are all implementable in Matlab linked to dSPACE, via FPGA or a microcontroller of a high processing frequency. The open power switch fault can be done by unplugging one of the PWM wires from the three phase inverter, so the switch will always receive a pulse with a zero value.

## References

[1] ZHANG, Y. and J. JIANG. Bibliographical review on reconfigurable fault-tolerant control systems. *Annual Reviews in Control*. 2008, vol. 32, iss. 2, pp. 229–252. ISSN 1367-5788. DOI: 10.1016/j.arcontrol.2008.03.008.

[2] ZHANG, J. and H. YUE. Fault Diagnosis and Fault-Tolerant Control in Power Plants and Power Systems. *Measurement and Control*. 2006, vol. 35, iss. 6, pp. 171–177. ISSN 0020-2940. DOI: 10.1177/002029400603900601.

[3] TABBACHE, B., M. BENBOUZID, A. KHELOUI, J.-M. BOURGEOT and A. MAMOUNE. An improved fault-tolerant control scheme for PWM inverter-fed induction motor-based EVs. *ISA Transactions*. 2013, vol. 52, iss. 6, pp. 862–869. ISSN 0019-0578, DOI: 10.1016/j.isatra.2013.07.004.

[4] RAISEMCHE, A., M. BOUKHNIFER, C. LAROUCI and D. DIALLO. Two Active Fault-Tolerant Control Schemes of Induction-Motor Drive in EV or HEV. *IEEE Transactions on Vehicular Technology*. 2014, vol. 63, iss. 1, pp. 19–29. ISSN 0018-9545. DOI: 10.1109/TVT.2013.2272182.

[5] HU, J.-S., D. YIN and Y. HORI. Fault-tolerant traction control of electric vehicles. *Control Engineering Practice*. 2011, vol. 19, iss. 2, pp. 204–213. ISSN 0967-0661. DOI: 10.1016/j.conengprac.2010.11.012.

[6] SLOTH, C., T. ESBENSEN and J. STOUSTRUP. Robust and fault-tolerant linear parameter-varying control of wind turbines. *Mechatronics*. 2011, vol. 21, iss. 4, pp. 645–659. ISSN 0957-4158. DOI: 10.1016/j.mechatronics.2011.02.001.

[7] FREIRE, N. M. A., J. O. ESTIMA, A. J. MARQUES CARDOSO. A New Approach for Current Sensor Fault Diagnosis in PMSG Drives for Wind Energy Conversion Systems. *IEEE*

*Transactions on Industry Applications*. 2014, vol. 50, iss. 2, pp. 1206–1214. ISSN 0093-9994. DOI: 10.1109/TIA.2013.2271992.

[8] JLASSI, I., S. KHOJET EL KHIL and N. MRABET BELLAAJ. Power switch and current sensor fault-tolerant control of PMSG drives for wind turbine systems. In: *10th International Symposium on Diagnostics for Electrical Machines, Power Electronics and Drives*. Guarda: IEEE, 2015, pp. 401–407. ISBN 978-1-4799-7743-7. DOI: 10.1109/DEMPED.2015.7303721.

[9] BENBOUZID, M. E. H., D. DIALLO and M. ZERAOULIA. Advanced Fault-Tolerant Control of Induction-Motor Drives for EV/HEV Traction Applications: From Conventional to Modern and Intelligent Control Techniques. *IEEE Transactions on Vehicular Technology*. 2007, vol. 56, iss. 2, pp. 519–528. ISSN 0018-9545. DOI: 10.1109/TVT.2006.889579.

[10] FERGANI, S., O. SENAME and L. DUGARD. A LPV/H∞ fault tolerant control of vehicle roll dynamics under semi-active damper malfunction. In: *American Control Conference*. Portland: IEEE, 2014, pp. 4482–4487. ISBN 978-1-4799-3274-0. DOI: 10.1109/ACC.2014.6859081.

[11] OUNNAS, D., M. RAMDANI, S. CHENIKHER and T. BOUKTIR. A Combined Methodology of H∞ Fuzzy Tracking Control and Virtual Reference Model for a PMSM. *Advances in Electrical and Electronic Engineering*. 2015, vol. 13, no. 3, pp. 212–222. ISSN 1336-1376. DOI: 10.15598/aeee.v13i3.1331.

[12] DJEGHALI, N., M. GHANES, S. DJENNOUNE and J.-P. BARBOT. Backstepping fault tolerant control based on second order sliding mode observer: Application to induction motors. In: *50th IEEE Conference on Decision and Control and European Control Conference*. Orlando: IEEE, 2011, pp. 4598–4603. ISBN 978-1-61284-801-3. DOI: 10.1109/CDC.2011.6161224.

[13] MEKKI, H., O. BENZINEB, D. BOUKHETALA and M. TADJINE. Fault Tolerant Control based Sliding Mode Application to Induction Motor. *IET Generation, Transmission & Distribution*. 2009, vol. 3, iss. 6, pp. 547–560. ISSN 1751-8687. DOI: 10.1049/iet-gtd.2008.0531.

[14] HUANG, G., Y.-P. LUO, C.-F. ZHANG, Y.-S. HUANG and K.-H. ZHAO. Current Sensor Fault Diagnosis Based on a Sliding Mode Observer for PMSM Driven Systems. *Sensors*. 2015, vol. 15, iss. 5, pp. 11027–11049. ISSN 1424-8220. DOI: 10.3390/s150511027.

[15] JASIM, A. H. and B. M. LAILA. Review on Fault Detection and Fault Tolerant Control Applied to Flight. *International Journal of Scientific Engineering and Research*. 2015, vol. 3, iss. 8, pp. 106–110. ISSN 2229-5518.

[16] JIANG, J. and X. YU. Fault-tolerant control systems: A comparative study between active and passive approaches. *Annual Reviews in Control*. 2012, vol. 36, iss. 1, pp. 60–72. ISSN 1367-5788. DOI: 10.1016/j.arcontrol.2012.03.005.

[17] SERON, M. M., X. W. ZHUO, J. A. DE DONA and J. J. MARTINEZ. Multisensor switching control strategy with fault tolerance guarantees. *Automatica*. 2008, vol. 44, iss. 1, pp. 88–97. ISSN 0005-1098. DOI: 10.1016/j.automatica.2007.05.024.

[18] LI, J., J. ZHOU, Z. YU and X. ZHU. Dual-fault tolerant control method of feedback loop for permanent magnet synchronous motor. In: *International Conference on Mechatronics and Automation*. Beijing: IEEE, 2015, pp. 459–463. ISBN 978-1-4799-7098-8 . DOI: 10.1109/ICMA.2015.7237529.

[19] TABBACHE, B., M. BENBOUZID, A. KHELOUI and J.-M. BOURGEOT. DSP-based sensor fault-tolerant control of electric vehicle powertrains. In: *International Symposium on Industrial Electronics*. Gdansk: IEEE, 2011, pp. 2085–2090. ISBN 978-1-4244-9312-8. DOI: 10.1109/ISIE.2011.5984482.

[20] ALKAYA, A. and I. EKER. Luenberger observer-based sensor fault detection: Online application to DC motor. *Turkish Journal of Electrical Engineering & Computer Sciences*. 2014, vol. 22, iss. 2, pp. 353–362. ISSN 1300-0632. DOI: 10.3906/elk-1203-84.

[21] WANG, H., S. PEKAREK and B. FAHIMI. Multilayer control of an induction motor drive:A strategic step for automotive applications. *IEEE Transactions on Power Electronics*. 2006, vol. 21, iss. 3, pp. 676–686. ISSN 0885-8993. DOI: 10.1109/TPEL.2006.872370.

[22] GAEID, K. S., H. W. PING, M. NASIR UDDIN, M. KHALID and A. SAGHAFINA. Wavelet based prognosis for fault tolerant control of induction motor with stator and speed sensor faults. In: *Industry Applications Society Annual Meeting*. Las Vegas: IEEE, 2012, pp. 1–8. ISBN 978-1-4673-0332-3. DOI: 10.1109/IAS.2012.6374029.

[23] OUACHTOUK, I., S. EL HANI and K. DAHI. Detection in Induction Machine. *Advances in Electrical and Electronic Engineering*. 2017,

vol. 15, no. 3, pp. 376–382. ISSN 1336-1376. DOI: 10.15598/aeee.v15i3.2193.

[24] KAMAL, E., A. AITOUCHE and M. OUEIDAT. Fuzzy Fault-Tolerant Control of Wind-Diesel Hybrid Systems Subject to Sensor Faults. *IEEE Transactions on Sustainable Energy*. 2013, vol. 4, iss. 4, pp. 857–866. ISSN 1949-3029. DOI: 10.1109/TSTE.2013.2253138.

[25] PERDUKOVA, D. and P. FEDOR. A Model-Based Fuzzy Control of an Induction Motor. *Advances in Electrical and Electronic Engineering*. 2015, vol. 12, no. 5, pp. 635–641. ISSN 1336-1376. DOI: 10.15598/aeee.v12i5.1229.

[26] ROTHENHAGEN, K. and F. W. FUCHS. Position estimator including saturation and iron losses for encoder fault detection of doubly-fed induction machine. In: *13th Power Electronics and Motion Control Conference*. Poznan: IEEE, 2008, pp. 1390–1397. ISBN 978-1-4244-1741-4. DOI: 10.1109/EPEPEMC.2008.4635462.

[27] AGUILERA, F., P. M. DE LA BARRERA and C. H. DE ANGELO. Behavior of electric vehicles and traction drives during sensor faults. In: *10th IEEE/IAS International Conference on Industry Applications*. Fortaleza: IEEE, 2012, pp. 1–7. ISBN 978-1-4673-2411-3. DOI: 10.1109/INDUSCON.2012.6453764.

[28] KIM, K.-C., S.-J. HWANG, K.-Y. SUNG and Y. KIM. A study on the fault diagnosis analysis of variable reluctance resolver for electric vehicle. In: *SENSORS*. Kona: IEEE, 2010, pp. 290–295. ISBN 978-1-4244-8169-9. DOI: 10.1109/ICSENS.2010.5689869.

[29] BOUROGAOUI, M., I. JLASSI, S. KHOJET EL KHIL and H. BEN ATTIA SETHOM. An effective encoder fault detection in PMSM drives at different speed ranges. In: *10th International Symposium on Diagnostics for Electrical Machines, Power Electronics and Drives*. Guarda: IEEE, 2015, pp. 90–96. ISBN 978-1-4799-7743-7. DOI: 10.1109/DEMPED.2015.7303674.

[30] RAMSDEN, E. *Hall-effect sensors: theory and applications*. 2nd ed. Boston: Elsevier/Newnes, 2006. ISBN 978-0-7506-7934-3.

[31] FRADEN, J. *Handbook of modern sensors: physics, designs, and applications*. 4th ed. New York: Springer, 2010. ISBN 978-1-4419-6466-3.

[32] SEPE, R. B., C. MORRISON and J. M. MILLER. Fault-tolerant operation of induction motor drives with automatic controller reconfiguration. *Practical Failure Analysis*. 2003, vol. 3, iss. 1, pp. 64–70. ISSN 1864-1245. DOI: 10.1007/BF02717411.

[33] DIALLO, D., M. E. H. BENBOUZID and A. MAKOUF. A fault-tolerant control architecture for induction motor drives in automotive applications. *IEEE Transactions on Vehicular Technology*. 2004, vol. 53, iss. 6, pp. 1847–1855. ISSN 0018-9545. DOI: 10.1109/TVT.2004.833610.

[34] TABBACHE, B., N. RIZOUG, M. E. H. BENBOUZID and A. KHELOUI. A Control Reconfiguration Strategy for Post-Sensor FTC in Induction Motor-Based EVs. *IEEE Transactions on Vehicular Technology*. 2013, vol. 62, iss. 3, pp. 965–971. ISSN 0018-9545. DOI: 10.1109/TVT.2012.2232325.

## About Authors

**Mohamed BOUAKOURA** was born in Batna, Algeria. He received his M.Sc. degree in Control and Diagnosis of Electrical Systems in 2014 from the University of Batna 2. He is currently pursuing his Ph.D. studies at the same university. His research theme is the diagnosis and FTC of induction motor drives.

**Nasreddine NAIT-SAID** was born in Batna, Algeria. He received his M.Sc. degree in Industrial Electricity in 1993 and a Ph.D. degree in electrical engineering from the University of Batna, Algeria in 2003. Currently, he is a Full Professor at the Electrical Engineering Department, University of Batna 2. His research interests include the application of AI techniques and control in the field of electrical machines.

**Mohamed-Said NAIT-SAID** was born in Batna, Algeria. He received his M.Sc. in Electrical and Computer Engineering from the Electrical Engineering Institute of Constantine University, Algeria, in 1992. He received his Ph.D. degree in Electrical and Computer Engineering from the University of Batna in 1999. Currently, he is a Full Professor at the Electrical Engineering Department, University of Batna 2. His research interests include electric machines, drives control, and diagnosis.

**Adel BELBACH** was born in Batna, Algeria. He received his Engineering degree in Electrical machines in 2006 and M.Sc. degree in 2013 from the University of Batna 2. He is currently pursuing his Ph.D. studies at the same university. His research theme is the diagnosis and FTC of induction motor drives.

# Appendix A
# Nomenclature and symbols

| | |
|---|---|
| IM | Induction motor. |
| FDI | Fault detection and isolation. |
| AFTC | Active fault tolerant control. |
| IFOC | Indirect field oriented control. |
| V/f CL | Closed loop V/Hz control. |
| V/f OL | Open loop V/Hz control. |
| $\Omega$, $\Omega^*$ | Rotor speed, reference rotor speed. |
| $V_a^*, V_b^*, V_c^*$ | Reference voltages produced by the AFTC. |
| $v_{abc}$ | Three phase voltages. |
| $i_{abc}$ | Three phase currents. |
| $\omega_s$ | Stator electric speed. |
| $f_s$ | Stator currents frequency. |
| $T_s$ | Stator currents period. |
| $T$ | Sampling time. |
| $p$ | Number of pole pairs. |
| $\Omega_f/I_f$ | Speed /Current value provided by a faulty speed/current sensor. |
| $\tau_d$ | Time between two points from speed data to detect speed sensor fault. |
| $d_sw, d_si$ | Speed sensor fault and current sensor fault detection signals respectively. |
| $d_sps$ | Power switch detection signal. |
| $\vec{V}^*_{s\frac{V}{f}CL}$ | Reference voltage generated by V/f CL Control in "$\alpha\beta$" reference frame. |
| $\vec{V}^*_{s\frac{V}{f}OL}$ | Reference voltage generated by V/f OL Control in "$\alpha\beta$" reference frame. |
| $\vec{V}^*_{sIFOC}$ | Reference voltage IFOC in "$\alpha\beta$" reference frame. |
| $\theta_{\frac{V}{f}CL}$ | Angle between the V/f CL reference voltage vector and the "$\alpha$" axis. |
| $\theta_{IFOC}$ | Angle between the IFOC reference voltage vector and the "$\alpha$" axis. |
| $\varphi$ | Angle between the reference voltage vectors of IFOC and V/f CL. |
| $s$ | Laplace operator. |
| $i_{sd}$, $i_{sq}$ | Direct and quadrature stator currents on "dq" reference frame. |
| $\phi_{rd}$, $\phi_{rq}$ | Direct and quadrature rotor fluxes on "dq" reference frame. |

# Appendix B
# Rated Data of the Induction Motor

**Tab. 2:** Rated data of the Induction Motor.

| Rated values | | Rated parameters | |
|---|---|---|---|
| Voltage ($\Delta/Y$) | 220/380 V | $R_s$, $R_r$ | 12.75, 5.1498 $\Omega$ |
| Current ($Y$) | 2.7 A | $L_s$, $L_r$, $M$ | 0.4991, 0.4331, 0.4331 H |
| Power | 0.9 kW | $J$ | 0.0035 kg·m$^2$ |
| Pole pairs ($p$) | 2 | $f$ | 0.001 Nm·rd$^{-1}$·s$^{-1}$ |

# Appendix C
# Simulation Specifications

All simulations are performed in Simulink/Matlab with a step size $T = 5 \cdot 10^{-6}$ s. Three phase inverter is composed of six ideal switches with antiparallel diodes and it is driven via PWM generator block of Simulink library. The DC voltage and carrier frequency are equal successively to 700 V and 6000 Hz. We used the IM model available in Simulink library with parameters of a 900 W motor. Reference voltages of IFOC are a "Sinus" function whereas those of V/f CL and V/f OL control are a "Cosinus" function. This is just a choice made at the beginning of this work and all calculations are built upon it. So if we change the "cosinus" function to "sinus" lookup tables and filters have to be readjusted.

To get closer to experiment, all simulations are performed in Matlab with an injected noise of a null average value and a variance of 1 rad·s$^{-1}$ and 0.1 A on speed and current data, respectively.

**Tab. 3:** IFOC and MRAS data.

| **IFOC and MRAS** |
|---|
| Speed controller: IP: integral=35, proportional=1 |
| $I_d$, $I_q$ current controllers: IP: integral=1000, proportional=250 |
| MRAS: PI: proportional=1000, integral=5000 |
| $\phi_r^* = 1$ Wb |

**Tab. 4:** Modified V/f CL control data.

| **V/f CL control (Fig. 12)** | | | | | |
|---|---|---|---|---|---|
| 1st order LPF: $\frac{1}{0.095s+1}$ | | | | | |
| $k_{d1} = 20$ | | | | | |
| $\tau_{d1} = 0.05$ | | | | | |
| PI controller: proportional= 0.8, integral= 3 | | | | | |
| 2nd order LPF: $\frac{60}{s^2+1.2\sqrt{60}s+60}$ | | | | | |
| $V_{boost} = 20$ | | | | | |
| **Lookup table** | | | | | |
| $\Omega^*$ [rad·s$^{-1}$] | 50 | 60 | 70 | 80 | 90 |
| Adaptive gain | 4.5 | 3.5 | 3 | 2.8 | 2.4 |
| 100 | 110 | 120 | 130 | 140 | 150 |
| 2.2 | 2 | 1.9 | 1.8 | 1.6 | 1.6 |

**Tab. 5:** Modified V/f OL control data.

| **V/f CL control (Fig. 13)** | | | | | |
|---|---|---|---|---|---|
| 1st order LPF: $\frac{1}{0.1s+1}$ | | | | | |
| $k_{d2} = 40$ | | | | | |
| $\tau_{d2} = 0.1$ | | | | | |
| $V_{boost} = 20$ | | | | | |
| **Lookup table** | | | | | |
| $\Omega^*$ [rad·s$^{-1}$] | 50 | 60 | 70 | 80 | 90 |
| $\tau$ [s] | 0.35 | 0.33 | 0.3 | 0.25 | 0.22 |
| 100 | 110 | 120 | 130 | 140 | 150 |
| 0.22 | 0.22 | 0.22 | 0.22 | 0.18 | 0.15 |